ORIGINAL RESEARCH

Recombinant epidermal growth factor-like domain-1 from coagulation factor VII functionalized iron oxide nanoparticles for targeted glioma magnetic resonance imaging

Heng Liu,[1,2] Xiao Chen,[1] Wei Xue,[1] Chengchao Chu,[2] Yu Liu,[2] Haipeng Tong,[1] Xuesong Du,[1] Tian Xie,[1] Gang Liu,[2] Weiguo Zhang[1,3]

[1]Department of Radiology, Institute of Surgery Research, Daping Hospital, Third Military Medical University, Chongqing, [2]State Key Laboratory of Molecular Vaccinology and Molecular Diagnostics, Center for Molecular Imaging and Translational Medicine, School of Public Health, Xiamen University, Xiamen, Fujian, [3]Chongqing Clinical Research Center for Imaging and Nuclear Medicine, Chongqing, People's Republic of China

Correspondence: Gang Liu
State Key Laboratory of Molecular Vaccinology and Molecular Diagnostics, Center for Molecular Imaging and Translational Medicine, School of Public Health, Xiamen University, Xiang'an South Road, Xiang'an District, Xiamen 361102, Fujian, People's Republic of China
Tel/fax +86 922 880 648
Email gangliu.cmitm@xmu.edu.cn

Weiguo Zhang
Department of Radiology, Daping Hospital, 10th Changjiang Road, Yuzhong District, Chongqing 400042, People's Republic of China
Tel +86 236 875 7621
Fax +86 236 875 7620
Email wgzhang01@163.com

Abstract: The highly infiltrative and invasive nature of glioma cells often leads to blurred tumor margins, resulting in incomplete tumor resection and tumor recurrence. Accurate detection and precise delineation of glioma help in preoperative delineation, surgical planning and survival prediction. In this study, recombinant epidermal growth factor-like domain-1, derived from human coagulation factor VII, was conjugated to iron oxide nanoparticles (IONPs) for targeted glioma magnetic resonance (MR) imaging. The synthesized EGF1-EGFP-IONPs exhibited excellent targeting ability toward tissue factor (TF)-positive U87MG cells and human umbilical vein endothelial cells in vitro, and demonstrated persistent and efficient MR contrast enhancement up to 12 h for preclinical glioma models with high targeting specificity in vivo. They hold great potential for clinical translation and developing targeted theranostics against brain glioma.

Keywords: epidermal growth factor-like domain-1, tissue factor, iron oxide nanoparticles, MRI, glioma

Introduction

Despite unprecedented efforts and recent advances in therapies, the prognosis remains poor for patients suffering from glioblastoma multiforme (GBM), the most aggressive form of glioma.[1] The patients experience a median survival of less than 15 months[2] and a 5-year survival rate of 3%–10%.[3] Accurate diagnosis of glioma is of great importance to preoperative delineation, surgical planning and survival prediction. However, the highly infiltrative and invasive nature of glioma cells often leads to blurred tumor margins, resulting in incomplete tumor resection and thus tumor recurrence.[4]

Among the various imaging techniques, magnetic resonance imaging (MRI) is the mainstay for clinical diagnosis of glioma due to its high temporal and spatial resolution.[5] Converging advances in the improved nanotechnology-based imaging probes and understanding of the molecular biology of tumor offer the opportunity to improve the visualization of brain tumor from normal tissues.[6–8] As negative MR contrast agents, iron oxide nanoparticles (IONPs) have attracted tremendous attention for glioma imaging due to their tunable sizes, large surface areas, easy modification and considerable biocompatibility.[9] Compared with gadolinium-based contrast agents used in clinic, IONPs can offer prolonged delineation of disseminated tumor boundaries due to their enhanced cellular uptake and slower elimination from tumor, mediated by
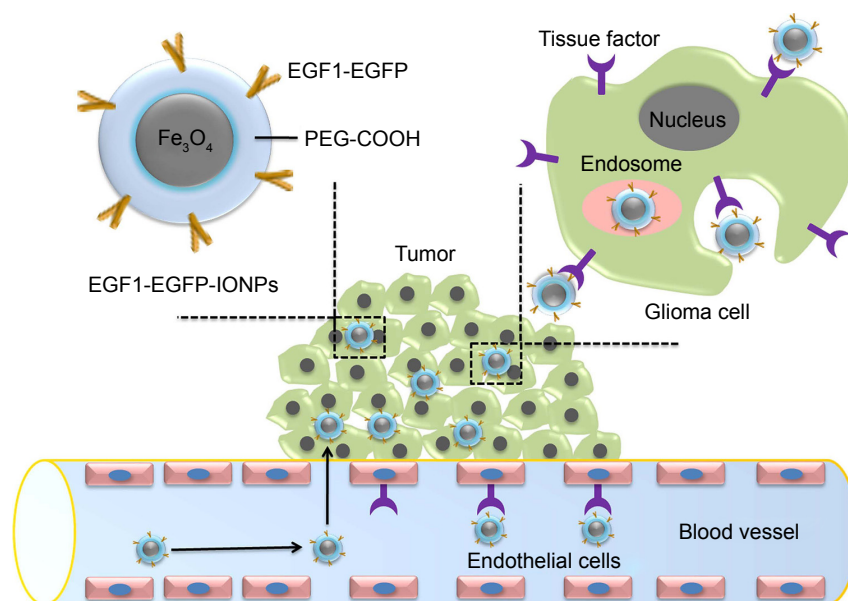
Figure 1 Schematic representation of EGF1-EGFP-IONPs for glioma targeting. After being intravenously injected, the disrupted BBB and receptor-mediated endocytosis by TF-positive glioma cells and endothelial cells can provide specific retention of NPs in the tumor, resulting in MR contrast enhancement.
Abbreviations: EGF1, epidermal growth factor-like domain-1; EGFP, enhanced green fluorescent protein; IONPs, iron oxide nanoparticles; NPs, nanoparticles; TF, tissue factor; MR, magnetic resonance; BBB, blood-brain-barrier.

the well-known enhanced permeability and retention (EPR) effect. Nevertheless, a major challenge faced with IONPs in tumor diagnosis is the nonspecific biodistribution and thus inability to target tumor sites. Tumor-specific IONPs are highly desirable for sensitive and accurate detection and delineation of glioma.

Tissue factor (TF) is a transmembrane glycoprotein that acts as the high-affinity receptor for coagulation factor VII (FVII) and the primary initiator of exogenous coagulation cascade and intracellular signaling.[10–12] TF is aberrantly overexpressed on tumor neovasculature and glioma cells but little on normal cells.[13] Increased TF expression is closely associated with tumor neovascularization, growth, invasion and metastasis.[14,15] The key role of TF in tumor progression makes it a favorable target for glioma imaging and therapy.[16,17] As the natural ligand of TF, FVII has been widely explored as a targeting moiety to deliver various therapeutic agents for tumor treatment.[18–20] To avoid inducing coagulation response, active site-inactivated recombinant human FVIIa,[21–24] mutated FVII,[20,25] FVII light chain,[26] TF inhibitors and anti-TF antibodies[27,28] have also emerged as targeting ligands. Although these TF-targeted strategies have achieved promising results, the instability and stereo-hindrance effect due to their large molecular weight, potential immunogenicity and difficulty for production on large scales restrict their further application in clinical situations. Very recently, numerous studies have supported the important

role of the epidermal growth factor-like domain-1 (EGF1) from the light chain of FVII in TF binding and FVII/TF complex formation,[29–33] without triggering coagulation. Taking advantage of the TF-targeting property of EGF1, EGF1-EGFP (EGFP, enhanced green fluorescent protein) decorated poly(ethylene glycol)-PLGA (PEG-PLGA)[34–37] NPs have shown satisfactory targeting efficiency toward TF-overexpressed sites, and EGF1 may ideally function as the targeting moiety highly specific for glioma.

Herein, we report a targeting nanoprobe EGF1-EGFP-IONPs for enhanced visualization of glioma cells (Figure 1), with EGF1-EGFP as the targeting moiety and IONPs as the MR imaging compound. The targeting property of EGF1-EGFP-IONPs toward glioma was evaluated systematically in vitro and in vivo.

Materials and methods
Materials
Human glioma U87MG cell line and human umbilical vein endothelial cells (HUVECs) were obtained from the Type Culture Collection of the Chinese Academy of Sciences (Shanghai, People's Republic of China). Water-dispersible IONPs with amphiphilic polymer and carboxylated poly(ethylene glycol) (PEG-COOH) coating were purchased from Ocean NanoTech (Springdale, AR, USA). Anti-TF antibody was obtained from Santa Cruz Biotechnology Inc. (Dallas, TX, USA). BCA Protein Quantitation Kit, Cell Counting Kit-8

(CCK-8) and 4′,6-diamidino-2-phenylindole dihydrochloride were obtained from Beyotime Institute of Biotechnology (Jiangsu, People's Republic of China). Perls stain was obtained from Leagene Biotech Co., Ltd. (Beijing, People's Republic of China). N-hydroxysulfosuccinimide (sulfo-NHS), N-(3-dimethylaminopropyl)-N′-ethylcarbodiimide (EDC), as well as all other chemical reagents were purchased from (Sigma-Aldrich Co., St Louis, MO, USA).

Preparation of recombinant EGFI-EGFP fusion protein

The EGF1 domain was cloned from human FVII, and EGF1-EGFP fusion protein was expressed in *Escherichia coli* BL21 (DE3) cells. The cDNA and amino acid sequence of EGF1-EGFP fusion protein are shown in Figures S1 and S2, respectively. Protein was harvested and purified using affinity chromatography, followed by elution with stepwise gradient concentrations of imidazole (pH 8.0). The purified protein was concentrated with centrifugal filter devices, and then identified by 12% sodium dodecyl sulfate-polyacrylamide gel electrophoresis (SDS-PAGE) with EGFP serving as control. The protein was stored in buffer (20 mM Tris, 150 mM NaCl, 10% glycerol, pH 7.5) at −80°C.

Preparation of EGFI-EGFP-IONPs and EGFP-IONPs

To activate the reactive –COOH groups on IONPs for covalent conjugation, freshly prepared EDC (100 µL, 50 mg/mL) and sulfo-NHS solution (80 µL, 50 mg/mL) were added to IONPs (2 mL, 0.5 mg Fe/mL) dissolved in phosphate buffered saline (PBS, 0.01 M, pH 5.5), and the reaction mixture was vigorously stirred for 30 min. Then, excessive EDC and sulfo-NHS molecules were removed using a NAP-5 desalting column balanced with PBS (pH 7.4). The eluted IONPs with activated –COOH groups were mixed with EGF1-EGFP solution (200 µL, 1.5 mg/mL), and the reaction was carried out in dark for 4 h. Finally, the NPs were purified by a PD-10 desalting column[38] and kept in PBS solution at 4°C. The concentration of protein in the supernatant was determined using BCA assay kit, and EGF1-EGFP density on IONPs surface was calculated. Similarly, EGFP was coupled with IONPs using the same procedure.

Characterization of NPs

The morphology of plain IONPs, EGFP-IONPs and EGF1-EGFP-IONPs was observed under transmission electron microscope (TEM, H-7500; Hitachi, Tokyo, Japan).

The hydrodynamic diameter and zeta potential of NPs were measured by dynamic light scattering (DLS, Zetasizer Nano S-90; Malvern Instruments, Malvern, UK). Samples were dispersed in PBS at a concentration of 0.1 mg Fe/mL. The surface chemical properties of NPs were characterized by Fourier transform infrared spectroscopy (FTIR; Bruker, Karlsruhe, Germany). The T2 relaxivity of NPs was determined using a 7.0 T MR scanner (Biospec USR70/20; Bruker). The IONPs were diluted with various iron concentrations in the range of 0–1 mM. T2 relaxation times were obtained using a T2-map multi-slice multi-echo (MSME) sequence with the following parameters: repetition time (TR)/echo time (TE): 4,000/9.5 ms; echo image: 10; slice thickness: 0.5 mm; field of view (FOV): 2×2 cm; matrix: 256×256. T2 relaxivity was plotted against iron concentrations and calculated by a linear fit.

Cell viability assay

U87MG cells and HUVECs were seeded in a 96-well plate with 5,000 cells/well. After 24 h, each well was added with different concentrations of EGFP, EGF1-EGFP, plain IONPs, EGFP-IONPs and EGF1-EGFP-IONPs. The final concentrations of protein or iron were in the range of 0–50 µg/mL. After incubation for additional 24 h, 10 µL of CCK-8 reagent was added and incubated for 2 h before the absorbance was determined at 450 nm. Cell viability (%) was calculated as the absorbance percentage of untreated cells.

Cellular uptake assay

To evaluate the specific binding ability of EGF1-EGFP to TF-positive cells, U87MG cells and HUVECs were seeded in a 24-well plate with 2×10⁴ cells/well. After 24 h, cells were incubated with 1.2 µM of EGF1-EGFP or EGFP for another 6 h. After being washed with PBS and fixed with 4% paraformaldehyde (PFA), the cells were observed under a fluorescence microscope (Olympus Corporation, Tokyo, Japan).

To evaluate the efficacy of EGF1-EGFP-IONPs in targeting glioma cells and HUVECs, cellular uptake of NPs was visualized by Prussian blue staining. Approximately, 2×10⁴ U87MG cells or HUVECs were seeded in a 24-well plate and allowed to reach 70% confluence. Cells were then incubated with plain IONPs, EGFP-IONPs and EGF1-EGFP-IONPs (equivalent to an iron concentration of 50 µg/mL) for 12 h. After being washed twice with PBS and fixed with 4% PFA, cells were incubated in Perl's staining solution for 20 min. After washing twice with deionized water and counterstaining with nuclear fast red for 10 min, cells were examined under a microscope.

For in vitro cell MRI, 5×10^5 U87MG cells were seeded in a six-well plate and allowed to reach 90% confluence. Then cells were incubated with plain IONPs, EGFP-IONPs and EGF1-EGFP-IONPs at a concentration equivalent to 50 µg Fe/mL for 12 h. After being washed twice with PBS, cells were collected and resuspended in 200 µL of 1% low melting agarose. Cell MRI was performed using a 7.0 T scanner. T2-weighted MSME sequences were performed with the following parameters: TR/TE: 4,000/45 ms; matrix: 256×256; FOV: 40×40 mm²; slice thickness: 1 mm; averages: 2; echo image: 8; interval time of echoes: 9.5 ms. T2 relaxation time was calculated using a single exponential fitting of the echo train.

Orthotopic GBM xenograft model

BALB/c nude mice (male, 4–5 weeks old, 20±2 g) were supplied by the Department of Experimental Animals (Daping Hospital, Third Military Medical University, People's Republic of China). All animal experiments were performed in accordance with the protocol approved by the Committee for Animal Studies at Daping Hospital. These animals were cared for according to the Chinese National Guidelines for Animal Welfare. An orthotopic GBM model was established by intracerebral implantation of U87MG cells. Mice were anesthetized with 10% chloral hydrate and placed in a small animal stereotaxic apparatus. Then, ~1×10^6 U87MG cells suspended in 5 µL of PBS were injected into the right striatum region (3.75 mm deep, 2.0 mm lateral and 2.5 mm behind the bregma) of mouse with a microinjector. The injection was given slowly over a period of 5 min, and then the needle was kept in for 5 min and slowly withdrawn over another 5 min.

In vivo MRI

In vivo MRI procedures were performed 2 weeks after tumor inoculation, using a 7.0 T MR scanner. EGF1-EGFP-IONPs or EGFP-IONPs at a dose of 15 mg Fe/kg body weight were injected into glioma-bearing mice via the tail vein. Image acquisition was performed before and at different time points post-injection of NPs with the following imaging parameters: 1) T1 RARE sequence: TR/TE: 800/6.89 ms; averages: 8; slice thickness: 0.5 mm, FOV: 2.5×2.5 cm; matrix: 256×256; 2) Turbo RARE-T2 sequence: TR/TE: 4,000/45 ms; averages: 2; slice thickness: 0.5 mm, FOV: 2.5×2.5 cm; matrix: 256×256; 3) T2*-map multigradient echo sequence: TR/TE: 800/4.5 ms; echo image: 8; slice thickness: 0.5 mm; FOV: 2.5×2.5 cm; matrix: 256×256; flip angle: 50°. T2 relaxation time was measured with the same sized ROI on the same slice of T2*-map images. The change

of T2 relaxation time was obtained using the following formula: $(T2_{pre}-T2_{post})/T2_{pre}\times100\%$, where $T2_{pre}$ and $T2_{post}$ are the T2 relaxation time of tumor prior to and post-injection of NPs, respectively.

Histologic analysis

At 24 h post-injection of NPs, the mice were sacrificed under anesthesia, and perfused with 30 mL of 0.9% NaCl and 20 mL of 4% PFA solution. After fixing in PFA for 24 h, the tissues were paraffin-embedded, sectioned to a thickness of 5 µm and stained with Prussian blue for histologic analysis.

Statistical analysis

The data were expressed as mean ± standard deviation. Mean values were compared using Student's *t*-test, carried out using SPSS 19.0. *P*-value <0.05 was considered statistically significant.

Results and discussion
Preparation and characterization of NPs

IONP-based molecular imaging has received tremendous attention for early diagnosis and detection of brain tumors in recent years.[9] Various ligands with specific targeting abilities have offered unique opportunities for enhanced accumulation of IONPs and specificity to glioma, eg, RGD peptide,[39] chlorotoxin,[40] epidermal growth factor,[41] heat shock protein 70,[42] lactoferrin,[43,44] transferrin[45] and antibodies (anti-insulin-like-growth-factor binding protein 7 single domain antibody,[46] anti-vascular endothelial growth factor receptor 2[47]). The targeted IONPs could reduce T2 and T2* relaxation times, providing tumor-specific contrast on susceptibility-weighted images[44,48] or T2*-weighted images[41,42] for improved tumor delineation. Appropriate tumor-specific biomarkers and corresponding targeting moieties are essential for improving the imaging sensitivity and accuracy. The commercially available IONPs used in this study consist of a 20 nm Fe_3O_4 core and oleic acid, amphiphilic polymer and PEG-COOH coating. The PEG-COOH coating on the surface allows them to be functionalized with EGFP or EGF1-EGFP via condensation reaction. SDS-PAGE analysis (Figure S3) showed that the 33.8 kDa EGF1-EGFP was highly expressed in *E. coli* BL21 (DE3) cells. The free –COOH groups on IONPs were activated by EDC and formed amide bonds with the free –NH₂ groups on EGFP and EGF1-EGFP. Finally, stable suspensions of EGFP-IONPs and EGF1-EGFP-IONPs were obtained. The BCA assay showed that the amount of protein was 0.3 mg/1 mg of IONPs.

An ideal nanoprobe should possess the following characteristics: appropriate size, fine monodispersity and excellent
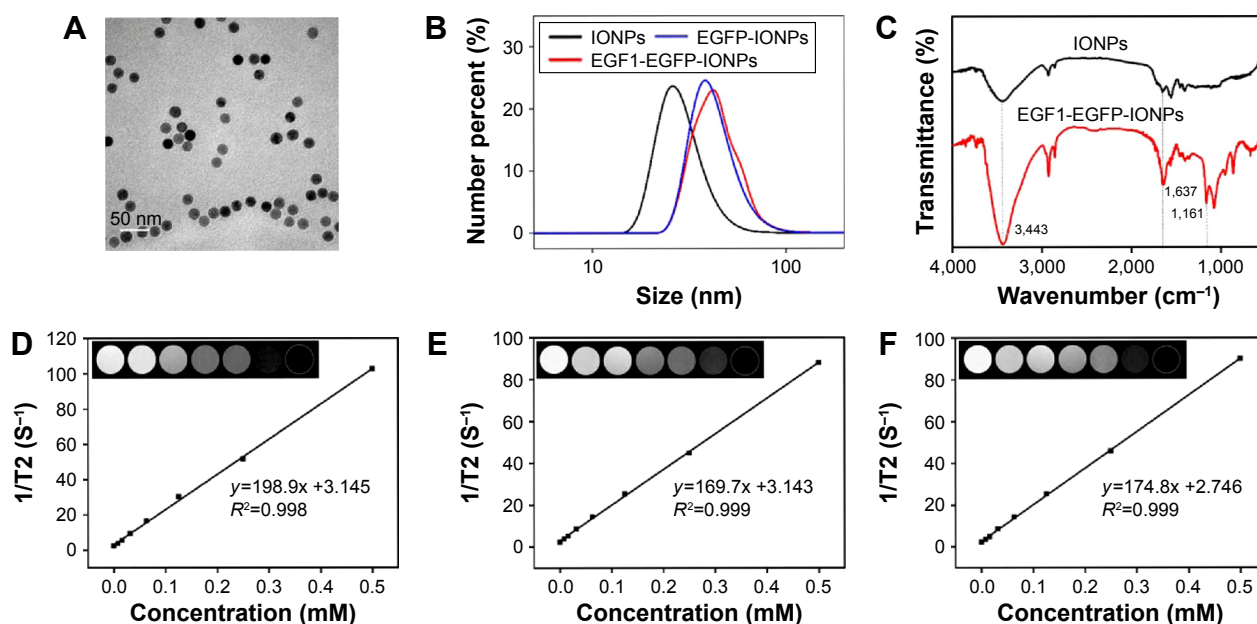
Figure 2 Characterization of NPs. TEM images of plain IONPs (**A**). Hydrodynamic sizes (**B**) and FTIR spectra (**C**) of NPs. T2 relaxation rate (1/T2, S⁻¹) of plain IONPs (**D**), EGFP-IONPs (**E**) and EGF1-EGFP-IONPs (**F**) in aqueous dispersion. Insets show corresponding T2-weighted phantom images with different concentrations of iron.
Abbreviations: EGF1, epidermal growth factor-like domain-1; EGFP, enhanced green fluorescent protein; IONPs, iron oxide nanoparticles; NPs, nanoparticles; TEM, transmission electron microscopy; FTIR, Fourier transform infrared spectroscopy.

magnetic properties. TEM (Figure 2A) showed that the plain IONPs were spherical in shape and monodisperse with uniform size of about 20 nm. The morphology of EGFP-IONPs and EGF1-EGFP-IONPs was similar to that of plain IONPs. The successful conjugation of IONPs with proteins was confirmed by DLS (Figure 2B). The hydrodynamic size was found to be 28.9±7.8, 42.8±8.5 and 44.5±8.6 nm for plain IONPs, EGFP-IONPs and EGF1-EGFP-IONPs, respectively. The zeta potential was −33.1±4.5, −26.3±4.2 and −23.9±4.8 mV for plain IONPs, EGFP-IONPs and EGF1-EGFP-IONPs, respectively (Figure S4). FTIR was also performed to characterize the coupling of proteins onto IONPs (Figure 2C). The stretching hydroxyl peak at 3,443 cm⁻¹ was observed on each IONP. There were several bands on nanoconjugates, which were absent on the plain IONPs. The strong peak located at 1,637 cm⁻¹ on nanoconjugates indicates the amide band formation. The band at 1,161 cm⁻¹ corresponds to the C–O vibrations. A broader O–H peak appeared on nanoconjugates, meaning that more hydroxyl bonds were formed. The results from DLS and FTIR suggested that proteins were successfully introduced. A phantom study was performed to evaluate the MRI contrast ability of NPs. The T2 signal decreased with increased iron concentration (Figure 2D–F). The T2 relaxivity (R2, 1/T2) value was calculated to be about 202, 173 and 178/mM/s for plain IONPs, EGFP-IONPs and EGF1-EGFP-IONPs, respectively. Although there was a slight reduction in T2 relaxivity

following conjugation due to the protection of proteins, EGF1-EGFP-IONPs would also meet the requirement as negative MR contrast agents.

Cell viability assay
The in vitro cytotoxicity of proteins and NPs on U87MG cells and HUVECs was determined using CCK-8 assay (Figure 3). No treatment demonstrated an obvious cytotoxic effect on U87MG cells and HUVECs in the studied concentration range. The viability of cells upon nanoconjugate treatment was slightly higher than that observed with plain IONP treatment under equivalent iron concentration, due to the protection of proteins. The results indicated low toxicity of EGF1-EGFP-IONPs.

Cellular uptake assay
TF was positive on U87MG cells, being about 30.5 times higher than that on HUVECs at the mRNA level (Figure S5), which was confirmed by immunofluorescent staining and real-time polymerase chain reaction analysis. EGF1-EGFP showed desired binding to U87MG cells and HUVECs (Figure 4A), and the fluorescence intensity was consistent with TF expression levels. However, the fluorescence in the EGFP group was quite negligible. To assess the specific cellular uptake of EGF1-EGFP-IONPs by TF-positive cells, Prussian blue staining was performed (Figure 4B). The blue granules in the cytoplasm indicated the presence of iron.
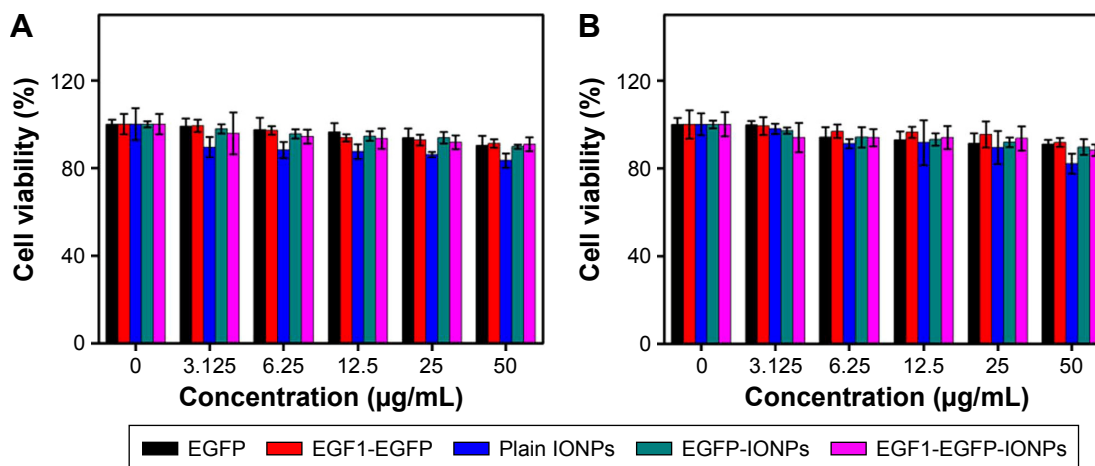
Figure 3 In vitro cell viability of U87MG cells (**A**) and HUVECs (**B**) after different treatments for 24 h.
Abbreviations: HUVECs, human umbilical vein endothelial cells; EGF1, epidermal growth factor-like domain-1; EGFP, enhanced green fluorescent protein; IONPs, iron oxide nanoparticles.

A much more significant uptake of EGF1-EGFP-IONPs was observed in U87MG cells after incubation for 12 h, and lower uptake was observed in HUVECs. However, no obvious blue staining was observed in the plain IONPs and EGFP-IONPs groups at the same iron concentration. The results corroborated cell binding assay, demonstrating the role played by EGF1-mediated targeting.

To confirm the targeting efficiency of NPs for MR contrast enhancement, cell MRI was performed after U87MG cells and HUVECs were treated with IONPs for 12 h. The cells treated with EGF1-EGFP-IONPs showed a significant negative contrast enhancement compared with untreated cells, while much less significant or even negligible contrast enhancement was observed at the same iron concentration in the plain IONPs and EGFP-IONPs groups (Figure 5A). The T2 relaxation time of the cells treated with

EGF1-EGFP-IONPs was significantly lower than that of cells treated with plain IONPs and EGFP-IONPs (P=0.000, Figure 5B). The results of cell MRI (Figure 5) and Prussian blue staining (Figure 4) suggested that EGF1 significantly enhanced the cellular uptake of NPs in TF-positive cells.

In vivo targeted MR imaging and accumulation assessment

The distribution of EGF1-EGFP in U87MG glioma in vivo demonstrated that a strong fluorescence intensity was observed in the tumor region, while negligible in healthy tissues, indicating the excellent targeting ability of EGF1-EGFP for glioma in vivo (Figure S6). The promising results prompted an investigation into the application of EGF1-EGFP-IONPs for in vivo targeted MR imaging of U87MG glioma-bearing mice. Neither any side effects nor behavioral
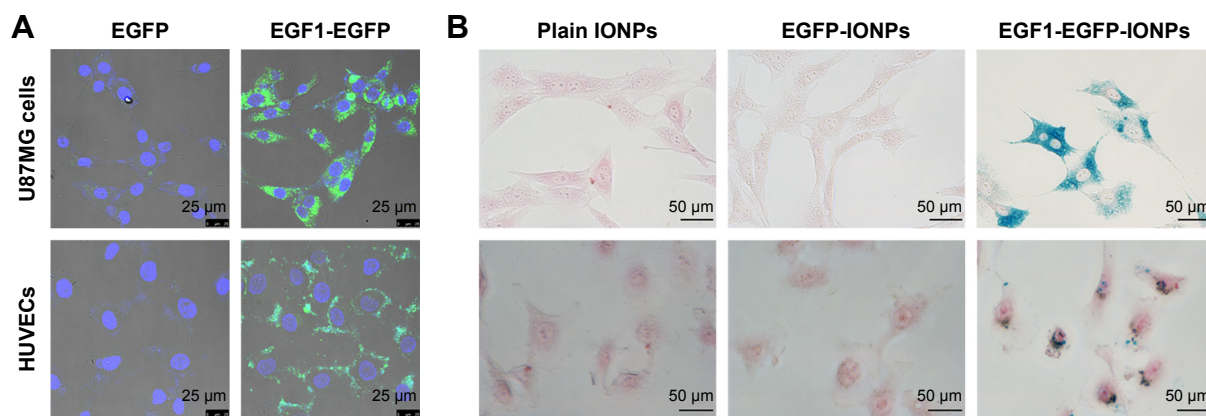
Figure 4 Targeting ability of EGF1-EGFP and EGF1-EGFP-IONPs in vitro. (**A**) Fluorescent images of U87MG cells and HUVECs incubated with EGF1-EGFP and EGFP. (**B**) Prussian blue staining of U87MG cells and HUVECs incubated with plain IONPs, EGFP-IONPs and EGF1-EGFP-IONPs. Magnification, ×400.
Abbreviations: EGF1, epidermal growth factor-like domain-1; EGFP, enhanced green fluorescent protein; HUVECs, human umbilical vein endothelial cells; IONPs, iron oxide nanoparticles.
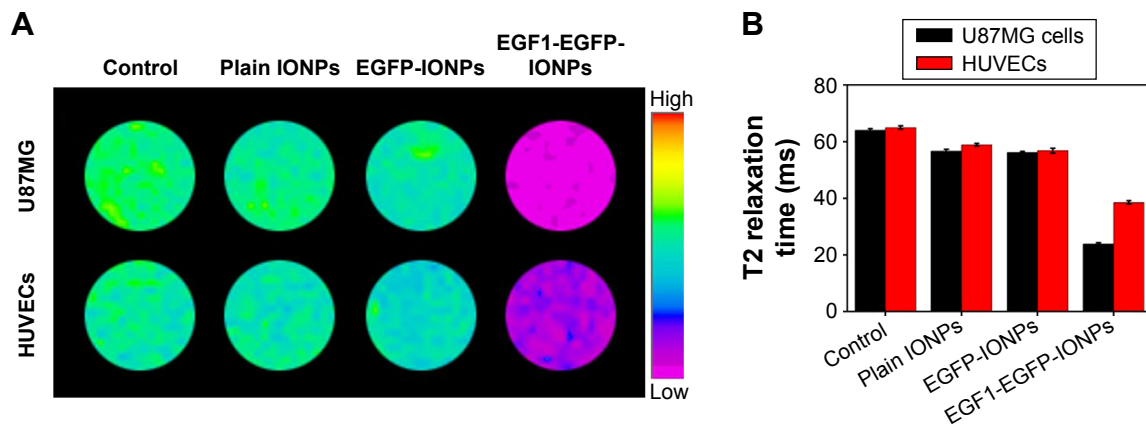
Figure 5 Cell MRI in vitro. T2-weighted images (**A**) and T2 relaxation time (**B**) of U87MG cells and HUVECs with control, plain IONPs, EGFP-IONPs and EGF1-EGFP-IONPs treatment (from left to right).
Abbreviations: EGF1, epidermal growth factor-like domain-1; EGFP, enhanced green fluorescent protein; HUVECs, human umbilical vein endothelial cells; IONPs, iron oxide nanoparticles; MRI, magnetic resonance imaging; ms, milliseconds.

abnormalities were observed after injection of IONPs, indicating the suitable and safe use of EGF1-EGFP-IONPs for application in vivo. Representative in vivo T2-weighted images of U87MG glioma-bearing mouse before and at different time points after administration of NPs are shown

in Figure 6A. The glioma presented as isointense and slightly hyperintense on T1- and T2-weighted images, respectively. Signal change on T2-weighted images is a good indicator for the existence of IONPs. After administration of EGF1-EGFP-IONPs, the T2 signal intensity in the tumor region
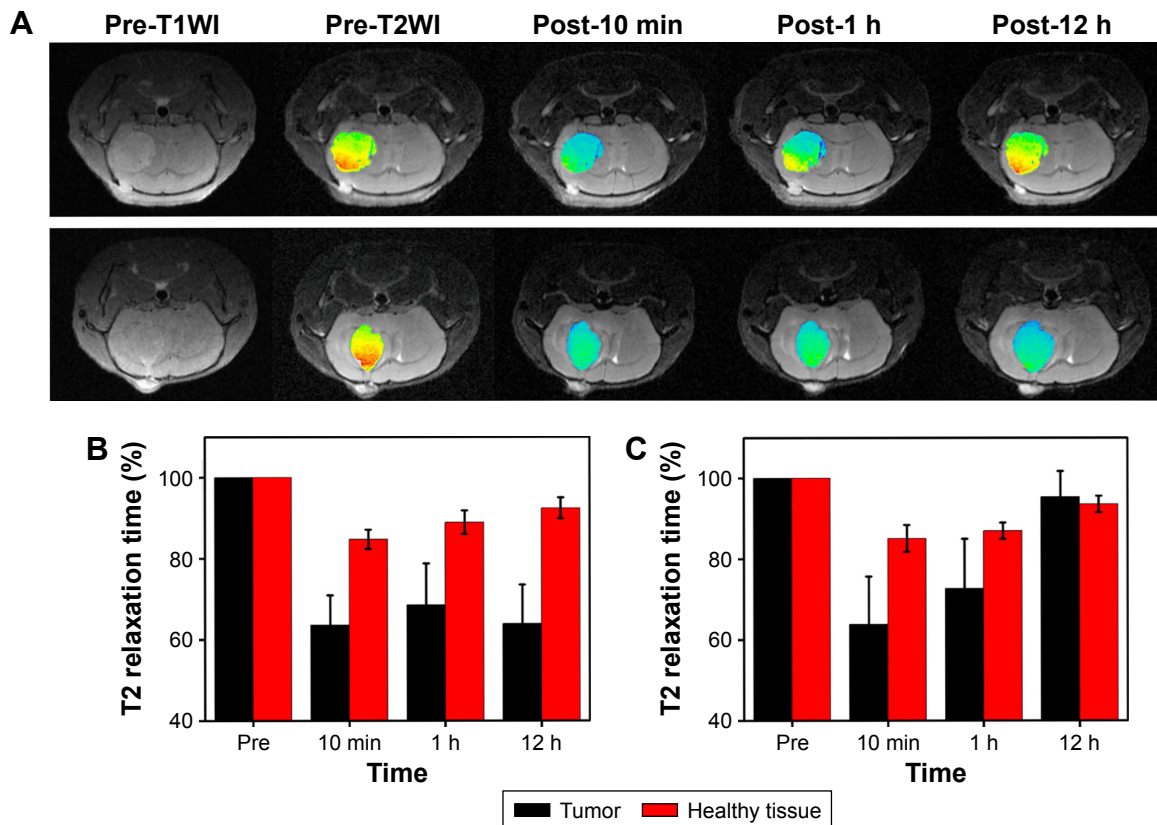
Figure 6 Representative in vivo T2-weighted images (**A**) and normalized T2 relaxation time (**B**, **C**) of mouse brain-bearing U87MG glioma before and at different time points post-injection of EGFP-IONPs (upper row, **C**) and EGF1-EGFP-IONPs (lower row, **B**).
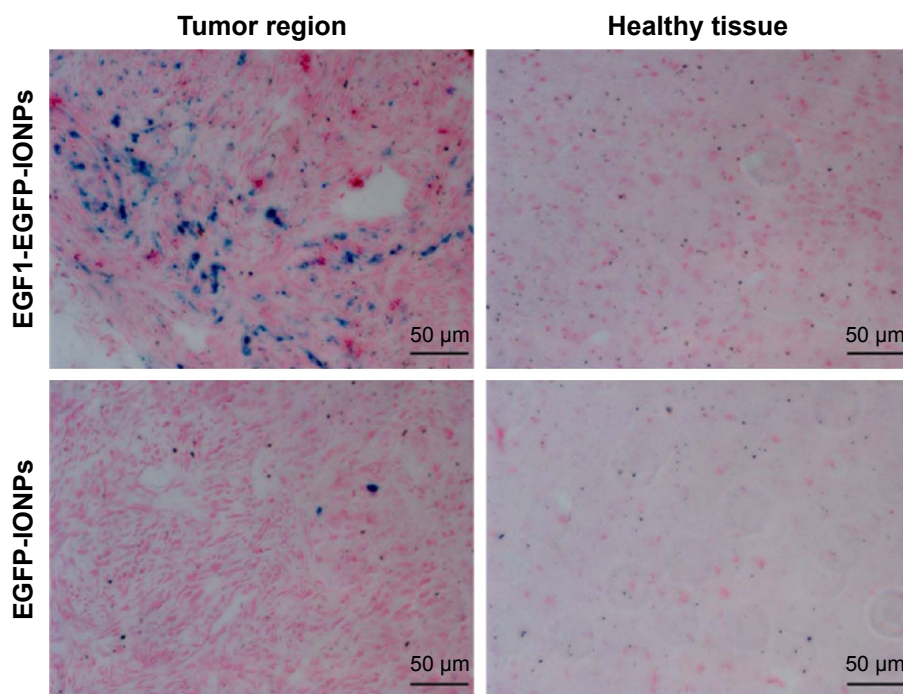**Abbreviations:** EGF1, epidermal growth factor-like domain-1; EGFP, enhanced green fluorescent protein; IONPs, iron oxide nanoparticles.

significantly decreased and remained at a lower level in comparison to that before injection. In the EGFP-IONPs group, the signal intensity gradually recovered during this period and was in proximity to that of baseline at 12 h post-injection. The T2 relaxation time in the tumor region was used for evaluation of the accumulation of NPs, quantified as a function of the post-injection time. It was found to be 22.9±3.1 ms prior to injection of NPs. To eliminate the influence of tumor T2 variation among mice, normalized T2 relaxation time was calculated by setting the time before injection as 100% (Figure 6B and C). As glioma suffers from high vasculature permeability, the relatively small-sized NPs can passively enter the tumor through leaky vasculature even without modification, dominated by the EPR effect. As expected, a significant decrease of T2 relaxation time in the tumor region was observed at 10 min post-administration for either EGFP-IONPs or EGF1-EGFP-IONPs. There was no significant difference at 10 min and 1 h post-injection between the two groups (P=0.969 and 0.559, respectively). Subsequently, the T2 relaxation time in the EGF1-EGFP-IONPs group remained at a relatively steady level, about 64% at 12 h post-injection. However, it gradually recovered over time in the EGFP-IONPs group, being 95.4% at 12 h post-injection. There was a statistically significant difference in normalized T2 relaxation time at 12 h post-injection of the targeted and non-targeted IONPs (P=0.000). It indicated that

EGF1-EGFP-IONPs could specifically and selectively bind to TF-positive cells and remained for up to 12 h in the tumor region, while the non-targeted EGFP-IONPs were gradually cleared out via further metabolic processes. The result suggests that in addition to the EPR effect, TF-mediated active targeting contributes to the improved accumulation of the targeted IONPs. The changes in the values of normalized T2 relaxation time in normal brain were much less compared to those in the tumor region at each time point. There was no statistical difference in normalized T2 relaxation time in normal brain at each time point between EGFP-IONPs and EGF1-EGFP-IONPs groups.

Prussian blue staining of brain tissue sections was performed at 24 h post-injection. Positive blue-stained iron particles were observed in the tumor region in the EGF1-EGFP-IONPs group (Figure 7), while negative results were observed in the EGFP-IONPs group. No positive staining was observed in healthy brain tissues in the two groups. Consistent with the results of MRI, Prussian blue staining confirmed the specific accumulation of NPs in the tumor region. Apparently, the MR negative contrast enhancement of glioma on T2-weighted images was due to the enhanced and specific accumulation of EGF1-EGFP-IONPs.

The prolonged shortening of T2 relaxation time by EGF1-EGFP-IONPs provides a long-time window for enhanced visualization of tumors on MRI, suggesting potential

Figure 7 Prussian blue staining of tumor and healthy brain tissues at 24 h post-injection of EGF1-EGFP-IONPs (upper row) and EGFP-IONPs (lower row). Magnification, ×200.
Abbreviations: EGF1, epidermal growth factor-like domain-1; EGFP, enhanced green fluorescent protein; IONPs, iron oxide nanoparticles.

implications for clinical applications. The NPs can help in noninvasive imaging of TF and monitoring the therapeutic effect of drugs that work through modulation of TF signaling. As TF is selectively overexpressed on tumor neovasculature and glioma cells, the synthesized NPs could improve diagnostic specificity and emerge as a predictive marker for glioma. Besides glioma, such NPs hold significant potential for targeted MR imaging of many other tumors and diseases where TF signaling is upregulated.

Although EGF1-EGFP-IONPs demonstrated persistent and efficient MR contrast enhancement of TF aberrantly expressing U87MG glioma in vivo, their long-term distribution, possible chronic toxicity, and elimination mechanism remain unclear, which require further verification. Considering the crucial role of TF in tumor progression, whether the introduction of EGF1 can block TF signaling and thus inhibit the biological behaviors of malignant glioma cells is the topic for further study. As glioma possesses high tumor heterogeneity, combining different targeting moieties aimed at multitargets for improving the diagnostic efficiency is also a good choice.

Conclusion

In summary, EGF1-EGFP-IONPs with excellent physicochemical properties were successfully synthesized and characterized. The as-prepared NPs demonstrated persistent and efficient MR contrast enhancement of TF-positive U87MG glioma with high targeting specificity in vivo. It holds great potential to identify the specific molecular subtypes of glioma, which may offer benefits for developing promising strategies (eg, molecular imaging, targeted therapy, therapeutic monitoring) for treating brain glioma in clinical setting.

Acknowledgments

Disclosure

References

1. Nano R, Lascialfari A, Corti M, et al. New frontiers for astrocytic tumours. *Anticancer Res*. 2012;32(7):2755–2758.
2. Wen PY, Kesari S. Malignant gliomas in adults. *N Engl J Med*. 2008; 359(5):492–507.
3. Linz U. Commentary on Effects of radiotherapy with concomitant and adjuvant temozolomide versus radiotherapy alone on survival in glioblastoma in a randomised phase III study: 5-year analysis of the EORTC-NCIC trial (*Lancet Oncol* 2009;10:459–466). *Cancer*. 2010; 116(8):1844–1846.
4. Stupp R, Mason WP, van den Bent MJ, et al. Radiotherapy plus concomitant and adjuvant temozolomide for glioblastoma. *N Engl J Med*. 2005;352(10):987–996.
5. Keunen O, Taxt T, Gruner R, et al. Multimodal imaging of gliomas in the context of evolving cellular and molecular therapies. *Adv Drug Deliv Rev*. 2014;76:98–115.
6. Wegscheid ML, Morshed RA, Cheng Y, Lesniak MS. The art of attraction: applications of multifunctional magnetic nanomaterials for malignant glioma. *Expert Opin Drug Deliv*. 2014;11(6):957–975.
7. Lopci E, Franzese C, Grimaldi M, et al. Imaging biomarkers in primary brain tumours. *Eur J Nucl Med Mol Imaging*. 2015;42(4):597–612.
8. Cheng Y, Morshed RA, Auffinger B, Tobias AL, Lesniak MS. Multifunctional nanoparticles for brain tumor imaging and therapy. *Adv Drug Deliv Rev*. 2014;66:42–57.
9. Liu H, Zhang J, Chen X, et al. Application of iron oxide nanoparticles in glioma imaging and therapy: from bench to bedside. *Nanoscale*. 2016; 8(15):7808–7826.
10. Chu AJ. Tissue factor, blood coagulation, and beyond: an overview. *Int J Inflam*. 2011;2011:367284.
11. Aberg M, Siegbahn A. Tissue factor non-coagulant signaling – molecular mechanisms and biological consequences with a focus on cell migration and apoptosis. *J Thromb Haemost*. 2013;11(5):817–825.
12. Falanga A, Marchetti M, Vignoli A. Coagulation and cancer: biological and clinical aspects. *J Thromb Haemost*. 2013;11(2):223–233.
13. Guan M, Jin J, Su B, Liu WW, Lu Y. Tissue factor expression and angiogenesis in human glioma. *Clin Biochem*. 2002;35(4):321–325.
14. Dutzmann S, Gessler F, Harter PN, et al. The pro-migratory and pro-invasive role of the procoagulant tissue factor in malignant gliomas. *Cell Adh Migr*. 2010;4(4):515–522.
15. van den Berg YW, Osanto S, Reitsma PH, Versteeg HH. The relationship between tissue factor and cancer progression: insights from bench and bedside. *Blood*. 2012;119(4):924–932.
16. Harter PN, Dutzmann S, Drott U, et al. Anti-tissue factor (TF9-10H10) treatment reduces tumor cell invasiveness in a novel migratory glioma model. *Neuropathology*. 2013;33(5):515–525.
17. Liu Y, Jiang P, Capkova K, et al. Tissue factor-activated coagulation cascade in the tumor microenvironment is critical for tumor progression and an effective target for therapy. *Cancer Res*. 2011;71(20):6492–6502.
18. Duanmu J, Cheng J, Xu J, Booth CJ, Hu Z. Effective treatment of chemoresistant breast cancer in vitro and in vivo by a factor VII-targeted photodynamic therapy. *Br J Cancer*. 2011;104(9):1401–1409.
19. Hu Z, Rao B, Chen S, Duanmu J. Targeting tissue factor on tumour cells and angiogenic vascular endothelial cells by factor VII-targeted verteporfin photodynamic therapy for breast cancer in vitro and in vivo in mice. *BMC Cancer*. 2010;10:235.
20. Hu Z, Garen A. Targeting tissue factor on tumor vascular endothelial cells and tumor cells for immunotherapy in mouse models of prostatic cancer. *Proc Natl Acad Sci U S A*. 2001;98(21):12180–12185.
21. Shoji M, Sun A, Kisiel W, et al. Targeting tissue factor-expressing tumor angiogenesis and tumors with EF24 conjugated to factor VIIa. *J Drug Target*. 2008;16(3):185–197.
22. Zhu S, Kisiel W, Lu YJ, et al. Visualizing cancer and response to therapy in vivo using Cy5.5-labeled factor VIIa and anti-tissue factor antibody. *J Drug Target*. 2015;23(3):257–265.
23. Zhu S, Kisiel W, Lu YJ, et al. Tumor angiogenesis therapy using targeted delivery of paclitaxel to the vasculature of breast cancer metastases. *J Drug Deliv*. 2014;2014:865732.

24. Sun A, Shoji M, Lu YJ, Liotta DC, Snyder JP. Synthesis of EF24-tripeptide chloromethyl ketone: a novel curcumin-related anticancer drug delivery system. *J Med Chem*. 2006;49(11):3153–3158.

25. Hu Z, Garen A. Intratumoral injection of adenoviral vectors encoding tumor-targeted immunoconjugates for cancer immunotherapy. *Proc Natl Acad Sci U S A*. 2000;97(16):9221–9225.

26. Zhang Q, Liu XJ, Hu L, et al. Factor VII light chain-targeted lidamycin targets tissue factor-overexpressing tumor cells for cancer therapy. *Int J Mol Med*. 2012;29(3):409–415.

27. Jiao JA, Kelly AB, Marzec UM, et al. Inhibition of acute vascular thrombosis in chimpanzees by an anti-human tissue factor antibody targeting the factor X binding site. *Thromb Haemost*. 2010;103(1):224–233.

28. Hong H, Zhang Y, Nayak TR, et al. Immuno-PET of tissue factor in pancreatic cancer. *J Nucl Med*. 2012;53(11):1748–1754.

29. Banner DW, D'Arcy A, Chene C, et al. The crystal structure of the complex of blood coagulation factor VIIa with soluble tissue factor. *Nature*. 1996;380(6569):41–46.

30. Pike AC, Brzozowski AM, Roberts SM, Olsen OH, Persson E. Structure of human factor VIIa and its implications for the triggering of blood coagulation. *Proc Natl Acad Sci U S A*. 1999;96(16):8925–8930.

31. Seetharam S, Murphy K, Atkins C, Feuerstein G. Cloning and expression of rat coagulation factor VII. *Thromb Res*. 2003;109(4):225–231.

32. Eigenbrot C. Structure, function, and activation of coagulation factor VII. *Curr Protein Pept Sci*. 2002;3(3):287–299.

33. Huile G, Shuaiqi P, Zhi Y, et al. A cascade targeting strategy for brain neuroglial cells employing nanoparticles modified with angiopep-2 peptide and EGFP-EGF1 protein. *Biomaterials*. 2011;32(33):8669–8675.

34. Shi W, Mei H, Deng J, et al. A tissue factor targeted nanomedical system for thrombi-specific drug delivery. *Biomaterials*. 2012;33(30):7643–7654.

35. Zhang B, Wang H, Liao Z, et al. EGFP-EGF1-conjugated nanoparticles for targeting both neovascular and glioma cells in therapy of brain glioma. *Biomaterials*. 2014;35(13):4133–4145.

36. Chen C, Mei H, Shi W, et al. EGFP-EGF1-conjugated PLGA nanoparticles for targeted delivery of siRNA into injured brain microvascular endothelial cells for efficient RNA interference. *PLoS One*. 2013;8(4):e60860.

37. Shi W, Mei H, Deng J, et al. The delivery of thrombi-specific nanoparticles incorporating oligonucleotides into injured cerebrovascular endothelium. *Biomaterials*. 2013;34(16):4128–4136.

38. Zhang F, Huang X, Zhu L, et al. Noninvasive monitoring of orthotopic glioblastoma therapy response using RGD-conjugated iron oxide nanoparticles. *Biomaterials*. 2012;33(21):5414–5422.

39. Luo Y, Yang J, Yan Y, et al. RGD-functionalized ultrasmall iron oxide nanoparticles for targeted T(1)-weighted MR imaging of gliomas. *Nanoscale*. 2015;7(34):14538–14546.

40. Sun C, Veiseh O, Gunn J, et al. In vivo MRI detection of gliomas by chlorotoxin-conjugated superparamagnetic nanoprobes. *Small*. 2008;4(3):372–379.

41. Shevtsov MA, Nikolaev BP, Yakovleva LY, et al. Superparamagnetic iron oxide nanoparticles conjugated with epidermal growth factor (SPION-EGF) for targeting brain tumors. *Int J Nanomedicine*. 2014;9:273–287.

42. Shevtsov MA, Yakovleva LY, Nikolaev BP, et al. Tumor targeting using magnetic nanoparticle Hsp70 conjugate in a model of C6 glioma. *Neuro Oncol*. 2014;16(1):38–49.

43. Zhou Q, Mu K, Jiang L, et al. Glioma-targeting micelles for optical/magnetic resonance dual-mode imaging. *Int J Nanomedicine*. 2015;10:1805–1818.

44. Abakumov MA, Nukolova NV, Sokolsky-Papkov M, et al. VEGF-targeted magnetic nanoparticles for MRI visualization of brain tumor. *Nanomedicine*. 2015;11(4):825–833.

45. Jiang W, Xie H, Ghoorah D, et al. Conjugation of functionalized SPIONs with transferrin for targeting and imaging brain glial tumors in rat model. *PLoS One*. 2012;7(5):e37376.

46. Tomanek B, Iqbal U, Blasiak B, et al. Evaluation of brain tumor vessels specific contrast agents for glioblastoma imaging. *Neuro Oncol*. 2012;14(1):53–63.

47. Towner RA, Smith N, Asano Y, et al. Molecular magnetic resonance imaging approaches used to aid in the understanding of angiogenesis in vivo: implications for tissue engineering. *Tissue Eng Part A*. 2010;16(2):357–364.

48. Blasiak B, Landry J, Tyson R, et al. Molecular susceptibility weighted imaging of the glioma rim in a mouse model. *J Neurosci Methods*. 2014;226:132–138.